frontiers | Frontiers in Materials

TYPE Original Research
PUBLISHED 19 June 2023
DOI 10.3389/fmats.2023.1202889

OPEN ACCESS

EDITED BY
Xin Zhang,
Southern University of Science and Technology, China

REVIEWED BY
Jun Xu,
Southeast University, China
Pei Li,
Xi'an Jiaotong University, China

*CORRESPONDENCE
Jiguo Zhou,
zhoujiguo@bcnu.edu.cn

RECEIVED 09 April 2023
ACCEPTED 23 May 2023
PUBLISHED 19 June 2023

CITATION
Zhou J, Wang G and Zhu G (2023), The durability of basalt-fiber-reinforced cement mortar under exposure to unilateral salt freezing cycles.
Front. Mater. 10:1202889.
doi: 10.3389/fmats.2023.1202889

The durability of basalt-fiber-reinforced cement mortar under exposure to unilateral salt freezing cycles

Jiguo Zhou*, Guihua Wang and Guangxing Zhu

School of Civil Engineering, Baicheng Normal University, Baicheng, China

Basalt fiber and cement-based materials have been widely applied in engineering structures. In this context, the durability of basalt-fiber-reinforced ordinary silicate mortar was systematically studied under exposure to unilateral salt freezing. The mechanical durability, chloride ion diffusion characteristics, and microscopic pore characteristics of cement mortar with basalt fiber content levels in the range of 0 kg/m^3–1.5 kg/m^3 were tested under exposure to 0–40 freeze–thaw cycles. The relationships of changes in the internal pore structure with mass loss, mechanical damage, and the physical properties of the material were also analyzed under exposure to salt freezing cycles. The results demonstrated that even a small amount of basalt fiber could significantly improve the mechanical properties of cement mortar under unilateral salt freezing and its resistance to salt freezing erosion. In particular, cement mortar with 1.2 kg/m^3 basalt fiber content exhibited good durability of compressive and flexural strength, while the specimens with no basalt fibers exhibited a relatively large degree of internal porosity under exposure to unilateral salt freezing. Our work provides concrete evidence for changes in the porosity of mortar under exposure to unilateral salt freezing, with these changes showing an exponential relationship with mortar mass loss and a strong linear correlation with changes in the compressive strength, flexural strength, and chloride ion diffusion coefficient of the material.

KEYWORDS

salt freezing effect, concrete durability, chloride ion diffusion, compressive strength, pore characteristics

1 Introduction

The durability of cement-based concrete structures is greatly affected by freeze–thaw action, ion corrosion, and dry–wet cycle action. More specifically, these actions generate a negative impact on the safety of use of cement-based structures during their design life (Hu et al., 2020). The mechanical and physical properties of a cement-based material structure will be damaged as working time increases under the action of road-defrosting salt or within a saline soil environment, as in the northeast region of China. It has been reported in the literature that freeze–thaw cycles (FTCs) lead inevitably to surface erosion in concrete and significantly decrease its compressive strength (Qiu et al., 2020). Basalt fibers have high mechanical strength, elevated thermal stability, and good alkali corrosion resistance (Dhand et al., 2015; Fiore et al., 2015). As a result, the prominent utilization of basalt fibers as synthetic fibers for engineering applications has attracted the attention of the scientific community during the last decade (Ahmed and Lim, 2021). Basalt fibers are currently used in

civil engineering materials because of their good mechanical and physical properties (Ahmad and Chen, 2018).

According to the literature, fiber-reinforced cement-based materials produce better engineering performance because the inclusion of basalt fibers into cement-based materials can improve the performance of the raw materials in engineering applications to a remarkable degree (Yan et al., 2019). This basalt-fiber-reinforced concrete is composed of cement-based composite materials. The basalt can improve the toughness of the cement mortar, and the impact of short basalt fibers is most significant (Ye et al., 2010). Various experimental studies reported on in the literature have demonstrated that the durability of the cement material structure can be significantly improved by the addition of an appropriate amount of basalt fiber, and the enhanced tensile properties and durability of basalt fiber can effectively improve the tensile resistance of the concrete (Hong et al., 2022). It has also been reported that the incorporation of basalt fiber into cement mortar or cement concrete in a particular proportion can also effectively improve the compressive and flexural strength of the material (Zhao et al., 2010; Rambo et al., 2015).

Pehlivanlı reported that the inclusion of fiber instead of quartz could increase the flexural and compressive strength of autoclaved aerated concrete, while reinforcement of autoclaved aerated concrete with basalt fibers can improve the fiber-related properties and adherence (Pehlivanlı et al., 2015). Katkhuda reported that the application of chopped basalt fibers minimally enhanced the compressive strength of recycled concrete, but significantly improved its flexural and splitting tensile strength (Katkhuda and Shatarat, 2017). In another interesting publication, Sun stated that concrete reinforced with 6-mm basalt fibers displayed better performance in terms of compressive and splitting tensile strength, and the maximum strength could be achieved with 2% basalt fibers (Sun et al., 2019). In addition, Wu studied the mechanical and microstructural properties of basalt fiber–slag powder–fly ash concrete (BF-SF-FAC), revealing that the use of 0.18% basalt fibers produced the best frost resistance, while the average chord length was identified as a primary factor in the amount of damage to the BF-SP-FAC (Wu et al., 2021). Su demonstrated that the use of basalt fibers had a greater impact than polypropylene fibers in terms of reducing the chloride content of concrete, and fractal dimension exhibited a strong positive correlation with the chloride diffusion coefficient (Su et al., 2022). Khan studied the influence of hybrid basalt fiber length and content on the properties of cementitious composites, and reported that the impact of reinforcement with four kinds of fibers of different lengths was far superior to that of reinforcement with single-length fibers at the same volume fraction (Khan and Cao, 2021). Zhang studied the mechanical properties of a new form of recycled concrete with basalt fibers incorporated. In this study, it was found that the mechanical properties of recycled concrete gradually improved at a replacement ratio of 50%, and the basalt fibers significantly improved the interface transition zone of the recycled concrete (Zhang et al., 2021).

Haidao investigated the behavior of homogeneous and hybrid self-consolidating concrete (SCC) mixtures fortified with basalt fibers, and found that the addition of basalt fibers played a notable role in improving the slant shear strength of hybrid concrete at elevated temperatures (Haido et al., 2021). Yang tested the surface strain field and tracked the development of surface cracks during a uniaxial compression test of basalt-fiber-reinforced concrete, reporting that adding an appropriate amount of basalt fiber can delay the early cracking of the concrete (Yang et al., 2021). Yavuz Bayraktar and colleagues examined the physico-mechanical and thermal properties and durability of basalt-fiber-reinforced foamed concrete, and verified the positive impact of basalt fibers with a high content of ground granulate blast furnace slag (GGBFS) on the compressive strength of foamed concrete specimens with a fly ash (FA) content of 100 kg/m^3 (Yavuz Bayraktar et al., 2021). Gencel conducted various experiments and proved that the incorporation of basalt fibers at 0%–3% content increased the flexural strength of foam concrete by up to 88%, whilee reducing drying shrinkage and increasing the integration of paste in the material (Gencel et al., 2022). Zhou and colleagues demonstrated that the inclusion of basalt fibers can significantly improve the toughness and crack resistance of concrete, and that the basalt fibers had a more pronounced impact on the tensile and flexural strength of the concrete than on its compressive strength (Zhou et al., 2020).

Based on the above-mentioned studies, it can be inferred that the macroscopic mechanical properties of basalt-fiber-reinforced concrete have been extensively examined in the literature (Kizilkanat et al., 2015; Jiao et al., 2019; Chen et al., 2021). Moreover, the application of basalt fibers in concrete and the corrosion resistance of basalt-fiber-reinforced concrete have been tested (Khan et al., 2021; Xiong et al., 2022). However, there are very few reports in the literature on the durability and model-building properties of basalt-fiber-reinforced concrete. Therefore, it is imperative to further study the relationships between the microstructural, physical, and mechanical properties of basalt-fiber-reinforced concrete. The underlying mechanism of reinforcement in basalt fiber cement-based materials should be thoroughly investigated to gain deep insights into their macromechanical and physical properties. At the same time, understanding the macroperformance of basalt-fiber-reinforced concrete in terms of its microstructural properties is extremely significant. From this perspective, in the present study, an extensive set of experiments was performed to study the frost resistance properties of fiber-reinforced cement mortar with basalt fiber content ranging from 0 kg/m^3 to 1.5 kg/m^3. The mechanical and physical properties of cement mortar specimens under unilateral freeze–thaw action were systematically investigated. The compressive strength, flexural strength, chloride ion diffusion properties, and microstructure of cement mortar specimens were tested, and the enhancing impact of basalt fibers on cement mortar under unilateral salt FTCs was analyzed. The relationships between the microscopic pore characteristics and macromechanical and physical changes in the basalt-reinforced cement mortar under the application of unilateral freeze–thaw action were examined. Additionally, the failure mechanism of basalt-fiber-reinforced mortar was studied.

2 Materials and methods

The binding material used in this study was 42.5 ordinary silicate white cement (Hebei Huaxue). China ISO standard sand (Xiamen Aisiou standard sand Co., Ltd.), with a particle size ranging from 0.08 mm to 2.0 mm, was used as the fine aggregate. A water-to-cement ratio of 0.5, with ordinary tap water, was used to mix the mortar, and high-strength basalt fibers with a length of 6 mm were mixed into the mortar. The properties of the cement and basalt fibers are presented in Table 1.

TABLE 1 Cement and basalt fiber properties.

Cement	Specific surface area (m^2/kg)	Initial setting time (min)	Final setting time (min)	Compressive strength at 28 d (MPa)
	400	123	185	42.8
Basalt fiber	Density (g/cm^3)	Tensile strength (N/tex)	Elastic modulus (GPa)	Fiber diameter (μm)
	2.8–3.3	0.41	100	17

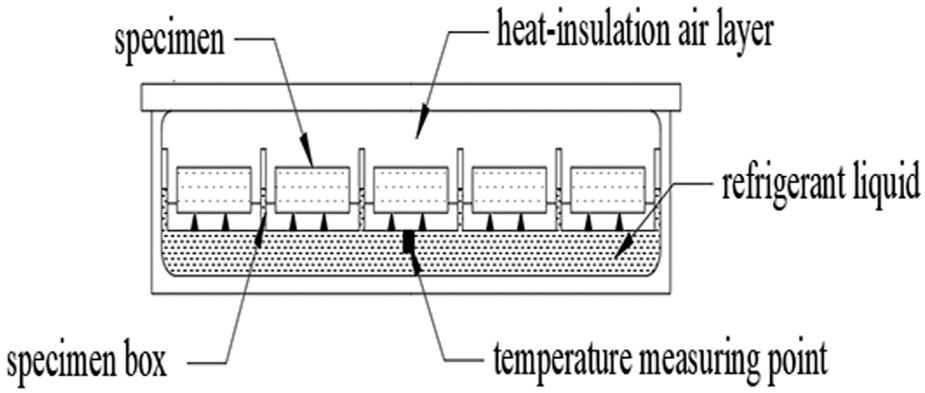

FIGURE 1
Unilateral salt freezing test chamber.

The mortar specimens were fabricated according to the ordinary concrete mechanical properties test method standard GB/T 50081-2002. Two sizes of mortar specimen were studied, namely, 70 × 70 × 70 mm^3 and 40 × 40 × 160 mm^3, with basalt fiber contents of 0% kg/m^3, 0.6 kg/m^3, 0.9 kg/m^3, 1.2 kg/m^3, or 1.5 kg/m^3. The cement mortar was cured at a humidity of 95% and an environmental temperature of 20°C ± 2°C. The initial mechanical properties were tested after 7 d and 28 d of curing. Subsequently, the specimens were placed into a unilateral freeze–thaw test chamber, as shown in Figure 1 in order to perform the durability test, and the mechanical properties, physical properties, and microscopic pore characteristics of each specimen were investigated after the specified number of FTCs. The freeze–thaw experiments were carried out according to the specified unilateral concrete freezing method of the Chinese Standard GB/T 50082–2009 (GB/T 50082-2009, 2019), and the mechanical experiments were carried out according to the Standard GB/T50081-2019 (GB/T50081-2019, 2019).

A YAW-300 concrete flexural compressive testing machine (Jinan Zhongluchang Testing Machine Manufacturing Co., Ltd.) was used to test the compressive and flexural strength of basalt-reinforced cement mortar. An HC-RCTF quick tester [Jianyan Huace (Hangzhou) Technology Co., Ltd.] was used to analyze the chloride ion concentration in each layer of the concrete material under freeze–thaw action in an NaCl solution. The MesoMR12-060H apparatus (Suzhou NIUMAG Analytical Instrument Corporation, Suzhou, China) was employed to investigate the microscopic porosity properties of basalt-fiber-reinforced mortar. An SU8010 positron emission scanning electron microscope (SEM) (Hitachi High-tech Company) was also used to examine the microstructural characteristics of the material, and an X'Pert III Powder X-ray powder diffraction machine (Malvern Panalytical Ltd., Eindhoven, Netherlands) was utilized to ascertain the composition of the material every 25 FTCs. The concrete specimens were analyzed by conducting XRD measurements using X'Pert III equipment. The samples were ground into a powder after the curing period for XRD analysis. C_uK_α radiation was recorded in the 2θ range of 10°–70° using a single-channel detector. Nuclear magnetic resonance (NMR) wave testing was conducted using the MesoMR12-060H instrument, with a magnetic field intensity of 0.3 ± 0.05 T. Finally, the Carr–Purcell–Meiboom–Gill (CPMG) sequence was used to characterize the lateral relaxation time spectra (T2) of the pore size of the concrete structure (Zhou et al., 2018).

3 Results and discussion

3.1 Changes in mechanical properties

In order to study the changes in the mechanical properties of the basalt-fiber-reinforced cement mortar specimens, the specimens were placed into a unilateral freeze–thaw test chamber to perform the freeze–thaw experiments after the 28-d standard curing period. Additionally, the mechanical properties of the specimens were investigated after every 10th freeze–thaw cycle. The pattern of changes in the compressive and flexural strength of specimens with varying basalt fiber content under the influence of unilateral freeze–thaw action in a salt solution is shown in Figure 2.

The mechanical properties of each type of mortar attained their maximum values after the specimens were cured for 28days.

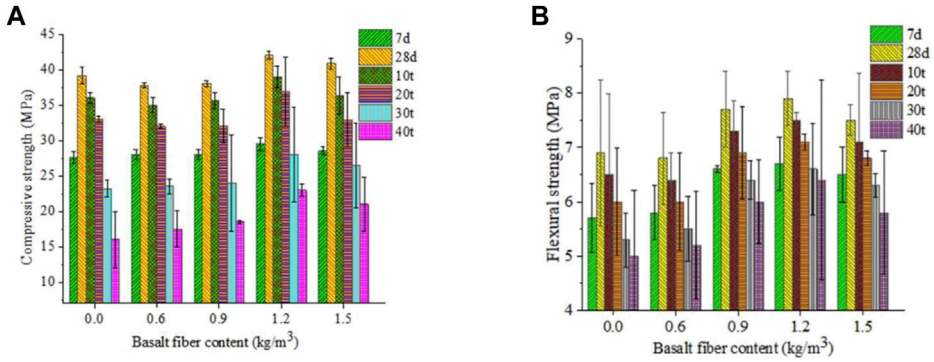

FIGURE 2
Changes in the mechanical properties of specimens with different levels of fiber content. **(A)** Compressive strength. **(B)** Flexural strength.

Interestingly, the specimens with added basalt fiber content ranging from 0.6 kg/m^3 to 1.5 kg/m^3 exhibited good mechanical persistence under unilateral freeze–thaw action in a salt solution. Compared to the mechanical properties of the specimens without any basalt fiber content, the average compressive strength of the specimens with basalt fiber content in the range 0.9 kg/m^3–1.5 kg/m^3 was increased by 3.86%, 2.89%, 2.73%, 2.83%, 12.72%, and 30.21%, and the flexural strength by 11.59%, 12.3%, 15.55%, 21.38%, and 21.33%, when the specimens were measured after curing for 7 d, after curing for 28d, and under the application of 10, 20, 30, and 40 unilateral FTCs, respectively. Compressive and flexural strength were highest in the specimens with a basalt fiber content of 1.2 kg/m^3, and those specimens had the highest values for these mechanical properties across all conditions in terms of the number of FTCs. Compared to the mechanical properties of the specimens with no basalt fiber content, the average compressive strength of the specimens with a basalt fiber content of 1.2 kg/m^3 increased by 6.88%, 7.27%, 8.33%, 11.82%, 20.68%, and 43.75%, and flexural strength by 17.54%, 14.49%, 15.38%, 18.33%, 24.52%, and 28%, when the specimens were measured after curing for 7 d, after curing for 28d, and under the application of 10, 20, 30, and 40 unilateral FTCs, respectively.

When the basalt-fiber-reinforced cement specimens were compared, it was observed that the specimens with a basalt fiber content of 0.9 kg/m^3–1.5 kg/m^3 exhibited superior mechanical properties to the others. The compressive and flexural strength of the specimens without added fibers were lower overall, and the durability of the mechanical properties of these specimens was inferior to that observed in the basalt-fiber-reinforced specimens. As per earlier reports, a small amount of basalt fiber can fill some pores of larger size, and the fibers overlapping each other can play a bridging role in ensuring the bonding force between the aggregate and cement mortar matrix. Therefore, an accurately calibrated level of basalt fiber content can enhance the strength of the structure (Chen et al., 2021). However, although the incorporation of fibers can play a bridging role, when basalt fibers are incorporated into the cement mortar at a content ratio greater than 1.2 kg/m^3, the incorporation of this much fiber destroys the original structural pores. The fibers are mixed together, and some fibers are stacked with each other. Thus, the increase in fiber content decreases the contact area between the fiber, aggregate, and cement mortar, leading to a decrease in matrix adhesion. As a result, the strength of cement mortar decreases as fiber content increases beyond 1.2 kg/m^3. Therefore, it can be inferred that the incorporation of a small proportion of basalt fiber into cement mortar produces improvement in its mechanical strength and mechanical durability under exposure to unilateral freezing, and the optimum basalt fiber content for enhanced compressive and flexural strength was determined to be 1.2 kg/m^3.

The results for compressive and flexural strength in the case of a 7-d curing period were found to be between the corresponding results for the specimens exposed to 20 and 30 FTCs. Although the results on compressive strength were similar for specimens with varying levels of basalt fiber content, they exhibited wide variation in flexural strength. The maximum difference from baseline in compressive strength was 6.8% for specimens with basalt fiber content in the range of 0.6 kg/m^3–1.5 kg/m^3, and the minimum difference was 1.44%. The maximum difference from baseline in flexural strength was 17.54% for specimens with basalt fiber content in the range of 0.6 kg/m^3–1.5 kg/m^3, and the minimum difference was 2.0%.

For the specimens tested after a 28-d curing period, both compressive and flexural strength showed an approximately linear decrease with an increasing number of unilateral freezing cycles, as shown in Figure 3. After 40 FTCs, the rate of loss of compressive and flexural strength was greater for the specimens with no basalt fiber content than for the specimens with basalt fiber content . Moreover, the specimens with varying levels of basalt fiber content exhibited major deterioration of their mechanical properties under 40 FTCs as compared with the specimens that only underwent the standard 28-d curing process. The compressive strength of the specimens with 0 kg/m^3, 0.6 kg/m^3, 0.9 kg/m^3, 1.2 kg/m^3, and 1.5 kg/m^3 basalt fiber content was decreased by 59.1%, 53.64%, 51.32%, 45.24%, and 48.59%, respectively. The flexural strength of the specimens with 0 kg/m^3, 0.6 kg/m^3, 0.9 kg/m^3, 1.2 kg/m^3, and 1.5 kg/m^3 basalt fiber content decreased by 27.54%, 23.53%, 22.07%, 18.98%, and 22.67%, respectively. Based on these results, it can be inferred that the mechanical properties in terms of compressive and flexural strength were superior in the case of the specimens with 1.2 kg/m^3 basalt fiber content, in comparison to the other specimens. Compared to the specimens without any

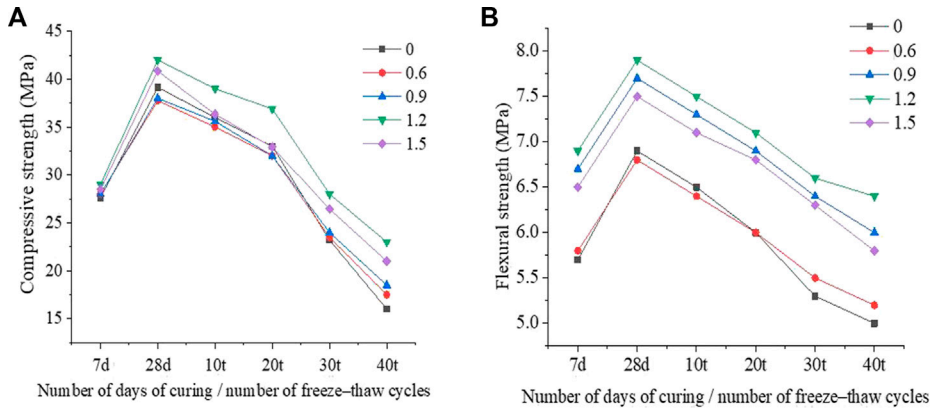

FIGURE 3
mechanical properties of specimens under exposure to different numbers of FTCs. **(A)** Compressive strength. **(B)** Flexural strength.

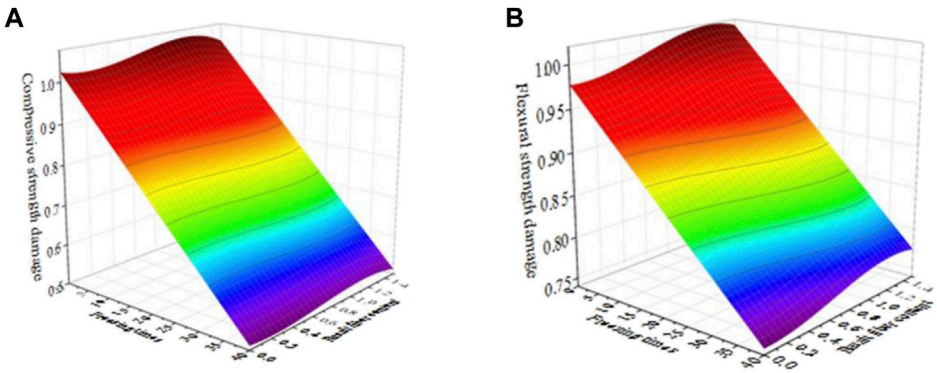

FIGURE 4
Models of mechanical damage. **(A)** Compressive strength. **(B)** Flexural strength.

basalt fiber content, the loss of compressive strength under exposure to 30 and 40 FTCs could be reduced on average by 13.74% and by 18.18%, respectively, and the loss of flexural strength loss could be reduced on average by 29.07% and by 22.85%, respectively, with the addition of 0.9 kg/m^3 to 1.5 kg/m^3 basalt fiber content. Hence, the incorporation of 0.6 kg/m^3–1.2 kg/m^3 basalt fiber content into these specimens resulted in improvements to their mechanical properties under exposure to an increasing number of FTCs.

Based on the results acquired on compressive and flexural strength and the ratio of compressive to flexural strength under exposure to FTCs for the specimens with varying basalt fiber content, the following expressions were constructed to fit the mechanical damage model:

$$\frac{f_c}{f_{cw}} = (m_c + n_c t)(a_c + b_c\rho + c_c\rho^2 + d_c\rho^3),$$
$$\frac{f_f}{f_{fw}} = (m_f + n_f t)(a_f + b_f\rho + c_f\rho^2 + d_f\rho^3),$$

where f_{cw} and f_{fw} are the compressive strength and flexural strength, respectively, of the cement specimens after a 28-d curing period. f_c and f_f represent the compressive strength and flexural strength, respectively, of the cement specimens under exposure to varying numbers of FTCs. Furthermore, t denotes the number of FTCs, m and n are weight coefficients for the FTCs, ρ is the basalt content, and a, b, c, and d are weight coefficients representing the influence of basalt fiber content on mechanical strength. The mechanical damage model for the compressive and flexural strength of cement specimens with basalt fiber content in the range of 0 kg/m^3–1.5 kg/m^3 under exposure to 0–40 FTCs can be derived based on regression analysis using the least squares method. The regression analysis models are presented in Figure 4.

It can be observed that the errors between the results of the strength test and the predictions of the model were within 10%, which proves that the accuracy of this model is well. The deterioration in compressive and flexural strength showed a strong linear relationship with the number of FTCs. Additionally, the degree of mechanical damage over 0–40 FTCs demonstrated a strong relationship in the form of a cubic parabola with level of basalt fiber content for cement mortar with basalt fiber content in the range of 0 kg/m^3 to 1.5 kg/m^3. Hence, the aforementioned values indicate the most suitable level of basalt fiber content for enhancing the compressive and flexural strength of basalt-reinforced mortar.

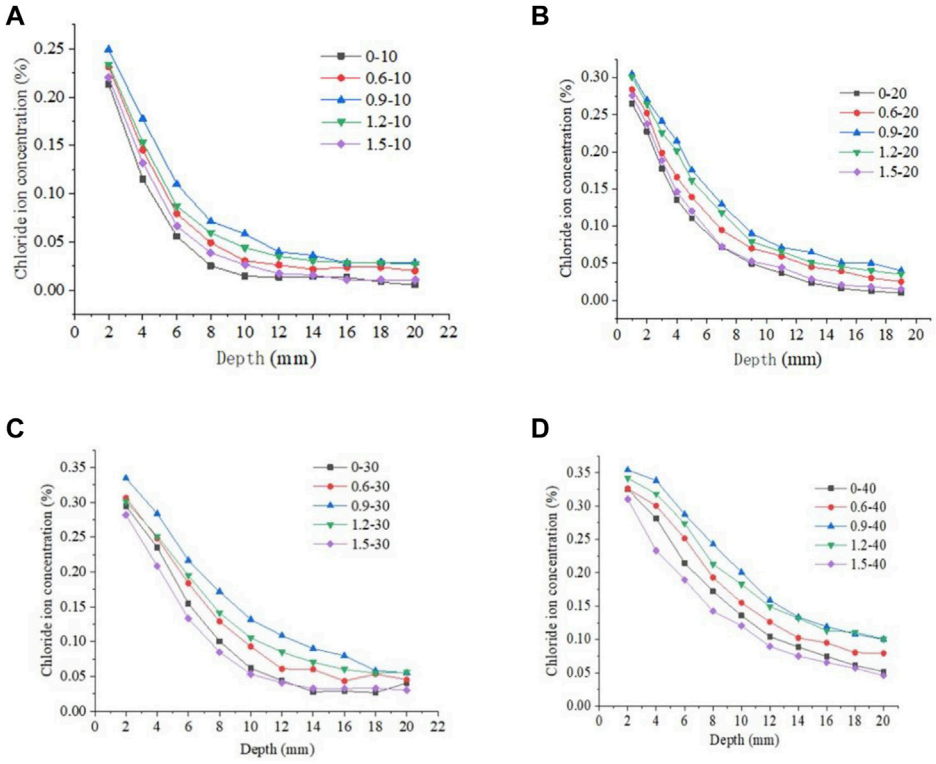

FIGURE 5
Changes in chloride ion concentration under exposure to **(A)** 10, **(B)** 20, **(C)** 30, and **(D)** 40 cycles of unilateral salt freezing.

3.2 Chloride ion diffusion properties

The chloride ion resistance of cement concrete has a direct influence on the corrosion-related characteristics of the steel bars inside the concrete structure (Yan, 2015). Chloride ion corrosion is the primary factor affecting the durability of a concrete structure, and the durability problems caused by chloride ions that induce erosion in marine environments have become a serious and arduous challenge in the field of civil engineering (Cao, 2013). Therefore, it is of major importance to study the characteristics of chloride ion diffusion in cement-based materials. In this study, the concentration of chloride ions inside the concrete was examined to investigate the influence of basalt fiber content on the resistance of each specimen to chloride ion diffusion inside the structure when 70 mm^3 × 70 mm^3 × 70 mm^3 specimens with different levels of basalt content were subjected to unilateral freeze–thaw action. The pattern of variation of the concentration of chloride ions inside the material at different depths from the erosion surface with the number of FTCs is shown in Figure 5.

The results indicated that the chloride ion diffusion concentration was essentially similar in specimens with different levels of basalt content. The results represented an exponential relationship between the change in chloride ion concentration and distance from the erosion surface. More specifically, chloride ion diffusion concentration under exposure to 10–20 FTCs was reduced, in descending order, for the specimens with 0.9 kg/m^3, 1.2 kg/m^3, 0.6 kg/m^3, 1.5 kg/m^3, and 0 kg/m^3 basalt content. Similarly, under exposure to 30–40 FTCs, the concentration was also reduced, in descending order, for the specimens with 0.9 kg/m^3, 1.2 kg/m^3, 0.6 kg/m^3, 0, and 1.5 kg/m^3 basalt content.

The mortar without added fibers was better able than specimens with a small amount of added fiber to resist chloride ion diffusion during the initial freeze–thaw stage, when the chloride ion concentration was lower in specimens without fiber than in specimens with fiber content. Compared to the specimen with no basalt fiber content, chloride ion concentration was increased by 96.45%, 179.12%, 146.89%, and 31.97%, on average, for the specimens with 0.6 kg/m^3, 0.9 kg/m^3, 1.2 kg/m^3, and 1.5 kg/m^3 fiber content, respectively, for an erosion distance in the range of 0–20 mm. This result indicates that although the incorporation an appropriate amount of basalt fiber into cement mortar can improve its compressive and flexural strength under exposure to unilateral FTCs, it has a negative impact on its resistance to chloride ion erosion. The ability of the mortar without basalt fiber content to resist chloride ion diffusion gradually decreased with an increasing number of FTCs. In addition, after 40 FTCs, the chloride ion concentration in the specimen without basalt fiber was higher than that in the specimen with 1.5 kg/m^3 basalt fiber content. In comparison to the specimen without basalt fiber, the chloride ion concentration in the range of 0–20 mm from the surface of the specimen increased by 19.88%, 48.55%, and 42.4% on average for the specimens with 0.6 kg/m^3, 0.9 kg/m^3, and 1.2 kg/m^3 basalt fiber content, respectively, and decreased by 12.2% for the specimen with 1.5 kg/m^3.

As can be observed from the experimental data obtained, the variation in chloride ion diffusion concentration with erosion

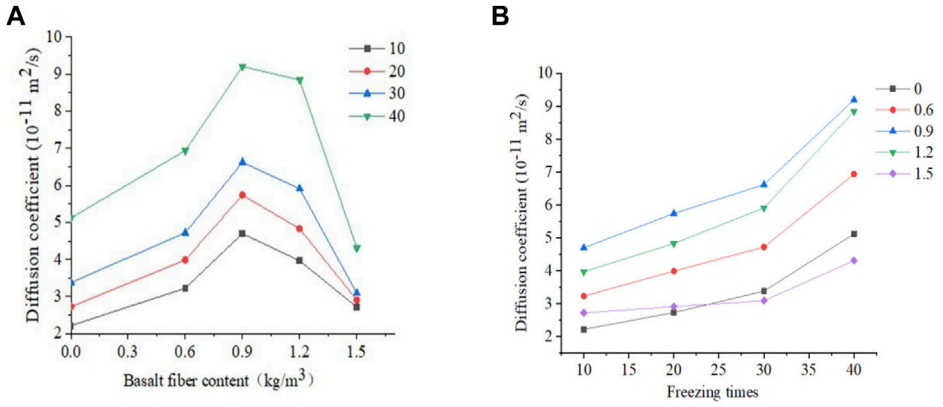

FIGURE 6
Variation in chloride ion diffusion coefficient for basalt-fiber-reinforced cement mortar. **(A)** Variation with basalt fiber content. **(B)** Variation with number of FTCs.

distance in the cement specimens took the form of an exponential relationship for specimens with different levels of basalt content under unilateral freeze–thaw action. The driving force of the diffusion of chloride ions was mainly the difference in concentration between the internal concrete and the external environment. Fick's second law can be applied to describe the process of chloride diffusion in saturated concrete (Zhang et al., 2010) and can be expressed by the following equation:

$$c(x,t) = C_0 + (C_s - C_0)\left[1 - erf\left(\frac{x}{2\sqrt{Dt}}\right)\right],$$

$$erf\left(\frac{x}{2\sqrt{Dt}}\right) = \frac{2}{\sqrt{\pi}}\int_0^z e^{-u^2}du,$$

where $C_{(x,t)}$ (%) is the chloride ion concentration at a depth of x from the erosion surface at the age of erosion t, C_0 (%) denotes the initial chloride ion content, C_s (%) represents the initial chloride ion content of the eroded surface, D (mm^2/s) represents the apparent chloride diffusion coefficient, x (mm) represents the erosion distance from the eroded surface, t (d) is the erosion age, and $erf(z)$ is the error function. On the basis of the experimental tests of chloride ion diffusion concentration in specimens with different levels of basalt fiber content under 0–40 FTCs, the chloride diffusion coefficient D for each specimen group, as calculated by Equation 2, is shown in Figure 6.

The goodness of fit measure R^2 for the chloride ion diffusion coefficients of basalt-fiber-reinforced cement mortar according to Fick's second law was above 0.9, which indicates that this law can be used to describe the properties of basalt fiber-reinforced cement mortar with respect to chloride ion diffusion under exposure to unilateral salt FTCs. The chloride ion diffusion coefficients of the specimens with basalt fiber increased with the number of unilateral FTCs, and an exponential growth law could be extracted for the relationship between chloride ion diffusion coefficient of and number of FTCs. Compared with the coefficient for specimens after 10 FTCs, the chloride ion diffusion coefficient increased by 22.97%, 23.53%, 22.13%, 21.66%, and 6.99% after 20 FTCs and by 130.63%, 114.86%, 95.74%, 122.6%, and 58.46% after 40 FTCs for the specimens with 0 kg/m^3, 0.6 kg/m^3, 0.9 kg/m^3, 1.2 kg/m^3, and 1.5 kg/m^3 basalt fiber content, respectively. Hence, it can be observed that the chloride ion diffusion coefficient of the different specimens increased with the number of FTCs. This is because the pores inside the cement specimens increased with the number of FTCs, which accelerated the diffusion of chloride ions in the structure.

The parabolic change exhibited extreme values for the chloride diffusion coefficient of each basalt-fiber-reinforced cement specimen under exposure to different numbers of FTCs. Under exposure to 10–40 unilateral FTCs, the chloride diffusion coefficient of specimens with a basalt fiber content of 0.9 kg/m^3 was greater than those of the other specimens with basalt fiber content in the range of 0 kg/m^3–1.5 kg/m^3. Compared to the specimen without basalt fiber, the chloride ion diffusion coefficient increased on average for specimens with a basalt fiber content of 0.6 kg/m^3–1.2 kg/m^3 by 78.68%, 77.78%, 70.12%, and 62.63% under exposure to 10, 20, 30, and 40 FTCs, respectively. Similarly, for the specimen with a basalt fiber content of 1.5 kg/m^3, the chloride ion diffusion coefficient increased by 22.52% and 6.59% under exposure to 10 and 20 FTCs, respectively, and decreased by 8.58% and 15.82% under exposure to 30 and 40 FTCs, respectively.

3.3 Change in pore characteristics

The mechanical and chloride ion diffusion properties of basalt-fiber-reinforced cement mortar were clearly altered under exposure to unilateral salt freezing. Hence, there was a need for further investigation of variation in the pores within the specimens under unilateral freeze–thaw action. Low-field nuclear magnetic resonance is a non-destructive testing method that has been widely used to examine the properties of cement-based materials (Xue et al., 2020; Xing et al., 2021). The method measures the variation in the transverse relaxation signal of the hydrogen atoms inside the material and obtains the intensity information corresponding to different transverse relaxation times. As a result, details of the variations in the pore size and pore proportion of the material can be derived (Dong et al., 2020). In this study, cement specimens

10.3389/fmats.2023.1202889

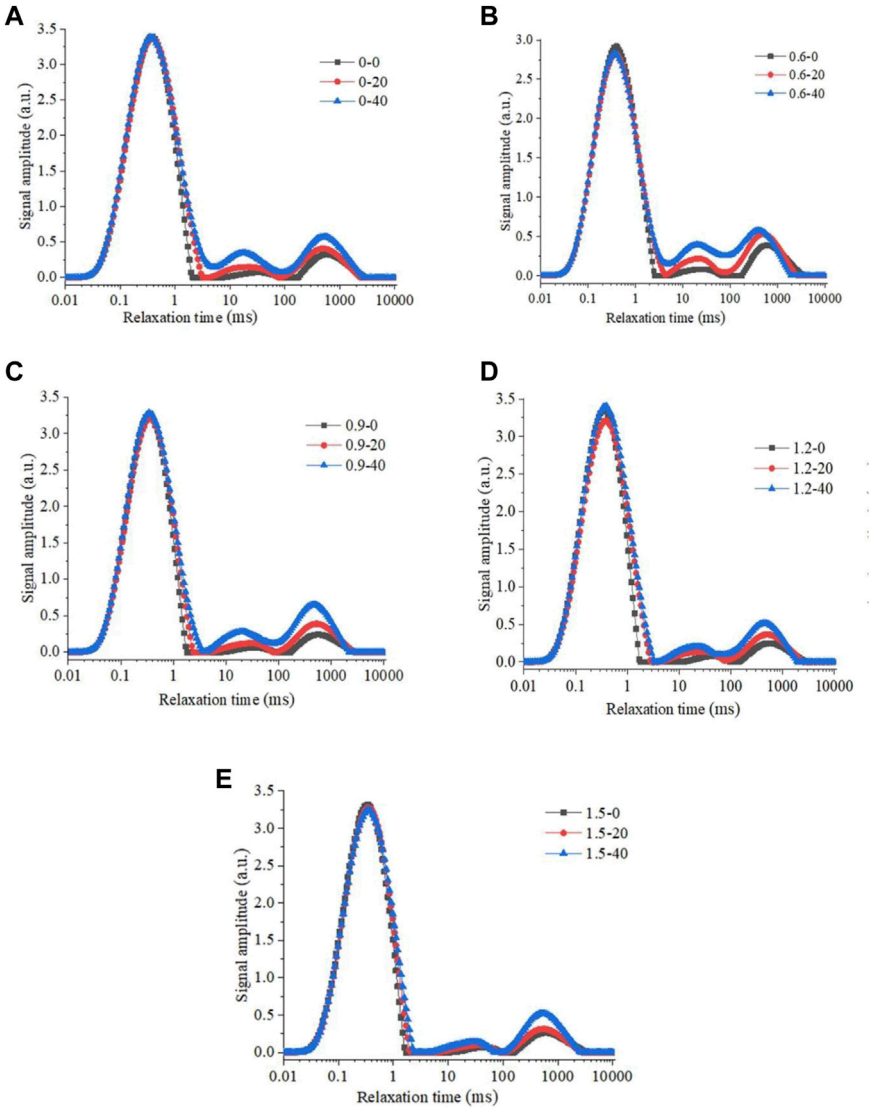

FIGURE 7
T2 spectra for basalt-fiber-reinforced cement mortar specimens with **(A)** 0 kg/m^3 basalt fiber content, **(B)** 0.6 kg/m^3 basalt fiber content, **(C)** 0.9 kg/m^3 basalt fiber content, **(D)** 1.2 kg/m^3 basalt fiber content, and **(E)** 1.5 kg/m^3 basalt fiber content.

with 0 kg/m^3–1.5 kg/m^3 basalt fiber content, cuboid in shape and 40 mm^3 × 40 mm^3 × 100 mm^3 in size, were initially tested after the standard 28-d maintenance and vacuum water retention process. Subsequently, the specimens were placed into a box for the experiment, in which they were subjected to unilateral FTCs. The T2 spectra of the specimens with different levels of basalt fiber content were measured using low-field nuclear magnetic resonance technology after 0, 20, and 40 FTCs; the variations observed in the T2 spectrum are presented in Figure 7. In the T2 spectrum plots, the horizontal coordinate represents relaxation time, which is an index of pore size inside the specimens, and the vertical coordinate represents the relaxation signal, which denotes the proportion of pores at each size inside the specimens.

As can be observed from the T2 spectrum per unit mass, the T2 spectrum of each specimen mainly presents three peaks, indicating that there were three main classes of pore size in the cement mortar. Each relaxation time of the T2 spectrum corresponds to a specific pore size: micropores and transition pores (<2.5 ms), middle-sized pores (2.5–100 ms), and large pores and cracks (>100 ms) (Lu et al., 2019). The greatest proportion of pores in the specimens were micro- and transition pores, which correspond to the first peak in the T2 spectrum. Relatively few pores fell into the categories of medium pores or macropores and cracks, which are denoted by the second and third peaks in the T2 spectrum, respectively. The strongest negative influence on the mechanical properties of cement is the presence of macropores and cracks, denoted by the third peak in the T2 spectrum. All component signals of the T2 spectrum gradually increased with the number of unilateral FTCs for specimens with different levels of basalt fiber content; this effect was not as clear for the increase in the first peak, but it was relatively clear for the increase in the second and third peaks. Thus, the proportion of medium pores and macropores and cracks in the

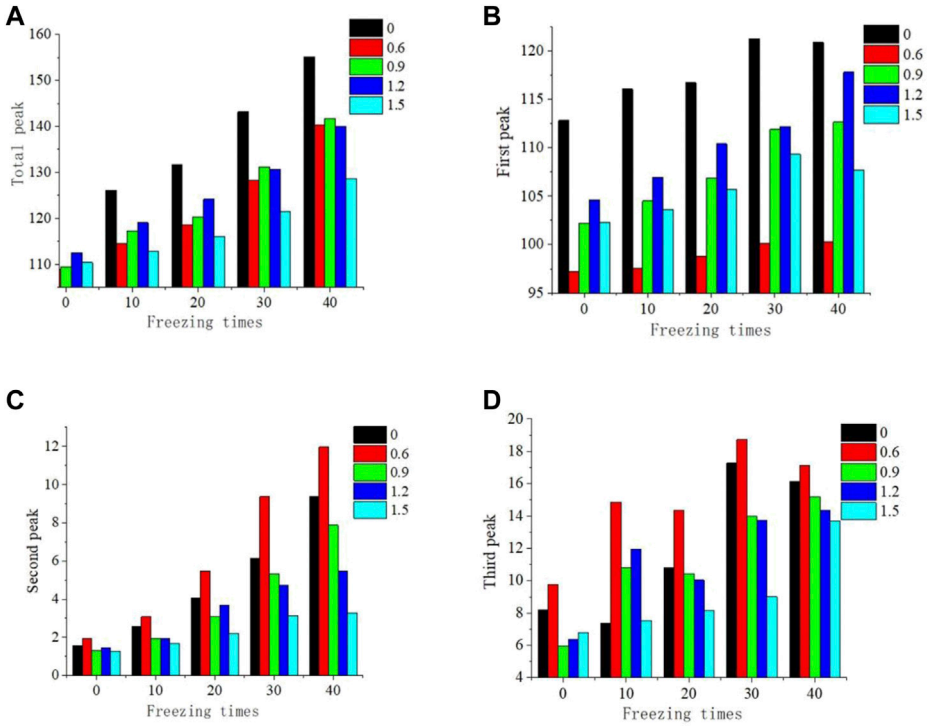

FIGURE 8
Variation in T2 spectrum peaks for mortar with basalt fiber. **(A)** Overall T2 spectrum signal. **(B)** First peak of the T2 spectrum. **(C)** Second peak of the T2 spectrum. **(D)** Third peak of the T2 spectrum.

structure was increased under exposure to unilateral FTCs. This outcome (i.e., the variable speed of increase of each peak in the spectrum) also indicates the different trends for each pore size in terms of its ratio to the total number of pores within the structure under an increasing number of FTCs. Under exposure to more FTCs, the proportion of micropores and transition pores gradually decreased, while the proportions of medium pores and of macropores and cracks gradually increased.

The T2 spectrum with the maximum total area was observed for the specimen without basalt fiber, and the minimum was observed for the specimen with 1.5 kg/m^3 basalt fiber content. In general, the total volume of the internal pores within the mortar without basalt fiber was the largest, while the volumes of internal pores were generally smaller within the mortar with basalt fiber were generally smaller than within those without fiber. Compared to the specimen without basalt fiber, the overall signal of the T2 spectrum was decreased by 11.19%, 10.74%, 8.28%, and 9.98% on average after 28-d standard curing, and by 9.75%, 8.15%, 7.44%, and 13.65% on average after exposure to 10–40 FTCs for the specimens with 0.6 kg/m^3, 0.9 kg/m^3, 1.2 kg/m^3, and 1.5 kg/m^3 basalt fiber content, respectively. The total number of peaks in the T2 spectrum gradually increased for each specimen with exposure to an increasing number of unilateral FTCs, which indicates that the number of pores within the specimens gradually increased with the continual action of unilateral salt freezing. Moreover, compared to the total volume of the pores within the specimens before freezing, the total volumes of pores within the structure increased by 7.38%, 8.98%, 9.98%, 10.39%, and 5.11% for specimens with 0 kg/m^3, 0.6 kg/m^3, 0.9 kg/m^3, 1.2 kg/m^3, and 1.5 kg/m^3 basalt fiber content, respectively, after 20 FTCs; the volume increased by 26.58%, 28.94%, 29.52%, 24.48%, and 16.61%, respectively, after 40 FTCs. Therefore, it can be concluded that the incorporation of an appropriate level of basalt fiber content into cement mortar can reduce the degree of porosity inside the material caused by internal damage under exposure to unilateral salt freezing.

Each peak area of the T2 spectrum increased with exposure to an increasing number of unilateral FTCs, as shown in Figure 8. Compared to the case before exposure to freezing, under exposure to 10–40 FTCs, for the cement specimens with 0.6 kg/m^3, 0.9 kg/m^3, 1.2 kg/m^3, and 1.5 kg/m^3 basalt fiber content, the first peak of the T2 spectrum indicates that micropores and transition pores inside the material increased by 5.24%, 2.06%, 6.64%, 6.90%, and 4.16% on average, respectively. Moreover, the second peak of the T2 spectrum signified that the volume of medium pores inside the material increased by 255.2%, 287.77%, 252.46%, 173.26%, and 105% on average, respectively, while the third peak of the T2 spectrum denoted that macropores and cracks inside the material increased by 57.62%, 66.69%, 111.99%, 96.62%, and 41.48% on average, respectively.

Each peak area of the T2 spectrum for the specimens with basalt fiber was not necessarily below that of the specimen without basalt fiber. The spectra for the specimen with no basalt fiber content were compared to those of the specimens with fiber content after the specimens were subjected to 10–40 unilateral salt freezing cycles. The first peak of the T2 spectrum indicated that the total micropores and transition pores inside the material was decreased by 15.95%,

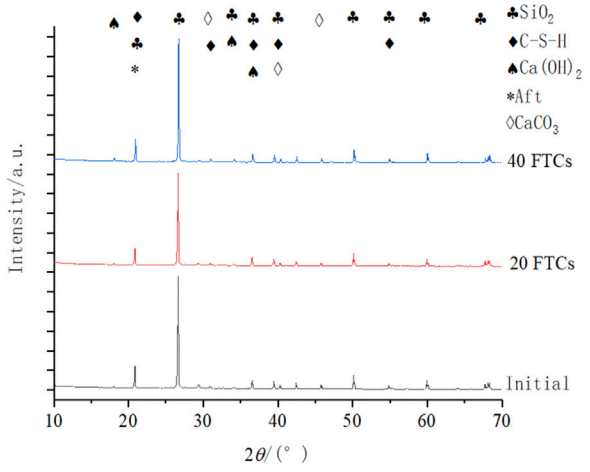

FIGURE 9
XRD spectra for a single specimen.

8.50%, 6.12%, and 10.08% on average for specimens with 0.6 kg/m^3, 0.9 kg/m^3, 1.2 kg/m^3, and 1.5 kg/m^3 basalt fiber content, respectively. The second peak of the T2 spectrum indicated that the total medium pores inside the material was decreased by 19.2%, 21.56%, and 43.04% for specimens with 0.9 kg/m^3, 1.2 kg/m^3, and 1.5 kg/m^3 basalt fiber content, respectively, but increased by 31.45% on average for the specimen with 0.6 kg/m^3 basalt fiber content. Finally, from the pattern in the third peak of the T2 spectrum, it can be inferred that macropores and cracks inside the material were decreased on average by 1.88%, 0.26%, and 20.44% for specimens with 0.9 kg/m^3, 1.2 kg/m^3, and 1.5 kg/m^3 basalt fiber content, respectively, but increased by 33.67% on average for the specimen with 0.6 kg/m^3 basalt fiber content.

As can be observed from the overall set of changes in micropores, transition pores, medium pores, macropores, and cracks occurring inside the basalt-reinforced cement specimens under exposure to unilateral salt freezing, the greatest rate of increase in the quantity of pores inside the structure was detected for the specimen with 0.9 kg/m^3 basalt fiber content. In the overall comparison, a reduced pore density inside the specimen with 1.5 kg/m^3 basalt fiber content was also detected. Beyond this, the increase in medium pores, macropores, and cracks was minimal for specimens with 0.9 kg/m^3–1.5 kg/m^3 basalt fiber content, demonstrating that the incorporation of an appropriate level of basalt fiber content in cement mortar could improve the resistance of structuresb to damage caused by unilateral freezing.

3.4 Composition and morphological properties

The specimens with 1.2 kg/m^3 basalt fiber content were experimentally tested using an X'Pert Ⅲ Powder X-ray powder diffractometer to analyze the characteristics of their composition under exposure to varying numbers of FTCs. The test powder was taken from the material within the specimen at a distance of 2 mm from the erosion surface after 20 and 40 FTCs, and the recorded XRD spectra are shown in Figure 9.

Based on the XRD spectra for the cement mortar, it can be observed that the main components of the material were gel (C-S-H), silica (SiO_2), calcium hydroxide ($Ca(OH)_2$), calcium carbonate ($CaCO_3$), and calcium sulphoaluminate hydrate (AFt/AFm). The salts gradually seeped into the interior of the structure, crystallized, and produced high crystallization pressure with an increasing number of FTCs. The composition of ettringite gradually increased under the continual action of these FTCs. In striking contrast, the composition of calcium hydroxide ($Ca(OH)_2$) decreased, and that of calcium carbonate ($CaCO_3$) gradually increased with NaCl seepage.

An SU8010 position emission scanning electron microscope (SEM) was employed to investigate the microstructure characteristics of the cement mortar specimens after unilateral salt freezing. The material with a 1.2 kg/m^3 basalt fiber content after 40 FTCs was used as a representative specimen. The SEM scanning images of this material are presented in Figure 10.

The basalt fiber bonded well with the slurry, the microstructure of the mortar was denser, and the use of an appropriate amount of fiber can enhance the mechanical properties of the mortar before the material is subjected to freeze–thaw action. The interface of the aggregate and basalt fibers remained smooth under continual exposure to FTCs, but the pores and cracks inside the structure were clearly detected through SEM imaging. The number and width of these cracks gradually increased, and cracks also appeared at the interface between the basalt fiber and cement mortar under exposure to freeze–thaw action. This result demonstrates that continual freeze–thaw action will result in the formation of micro-cracks within the structure and in detachment of the interface of the fibers with the cement slurry. As a result, the compressive and flexural strength of the material will be reduced, and the chloride ion diffusion coefficient will be increased. Therefore, the mechanical properties of the mortar will deteriorate, and their related physical properties will also be negatively affected.

3.5 Correlation between porosity and mass

The basalt-fiber-reinforced cement mortar specimens were subjected to water freeze–thaw action and salt erosion under unilateral salt freezing. Hydrostatic pressure, osmotic pressure, and expansion pressure are generated inside the structure under the action of pure water freeze–thaw, all of which cause damage to the performance of the concrete. Salt crystallization pressure also induces major damage to concrete structures when the material is subjected to freeze–thaw action under exposure to salt solution. Crystallization and osmotic pressure caused by a difference in salt concentration are also induced inside a structure when the material is subjected to multiple cycles of freeze–thaw action under exposure to salt solution, which result in cracking damage to the concrete(Xiaoping, 2013). Exfoliation occurs on the outer surface of the specimen, resulting in reduction of its mass as the number of FTCs increases. The pattern of variation in the mass loss of the specimens under exposure to unilateral salt freezing cycles is displayed in Figure 11.

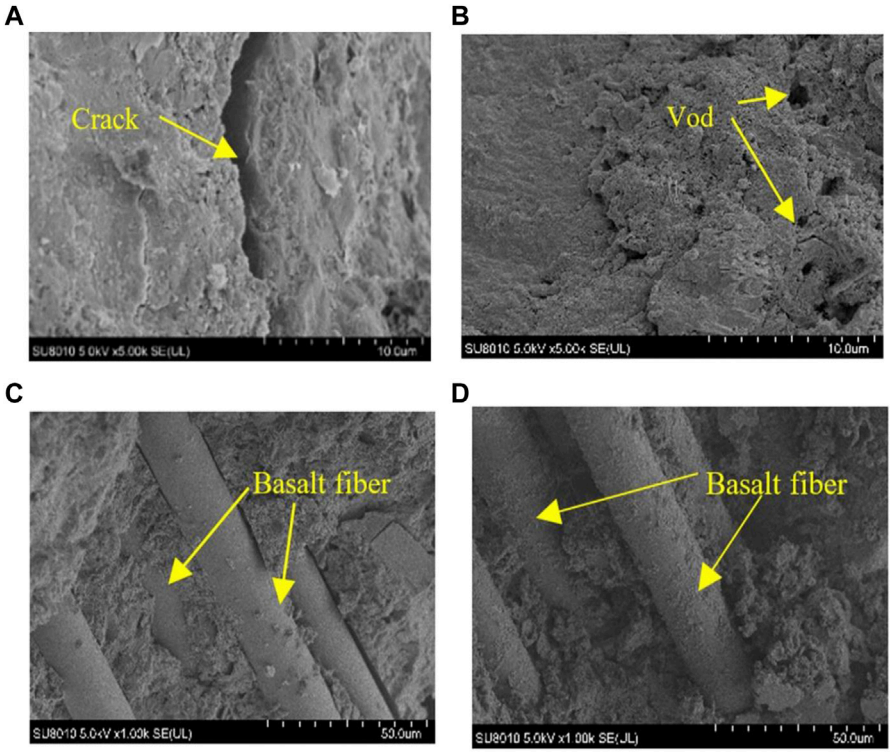

FIGURE 10
SEM scanning images of the specimen at **(A)** × 5,000; **(B)** × 5,000; **(C)** × 1,000; **(D)** × 1,000.

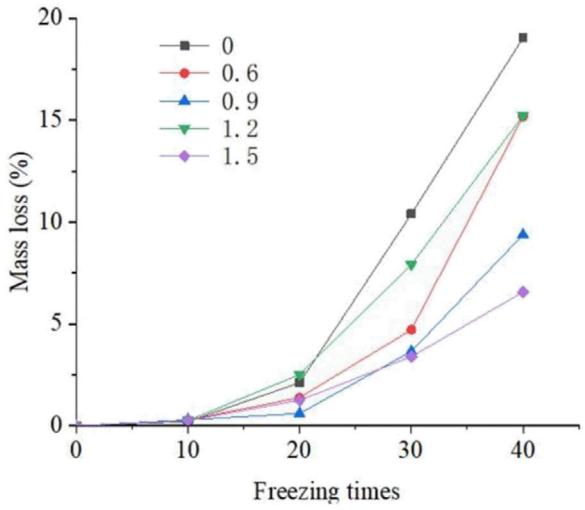

FIGURE 11
Loss of mass from specimens under exposure to salt freezing.

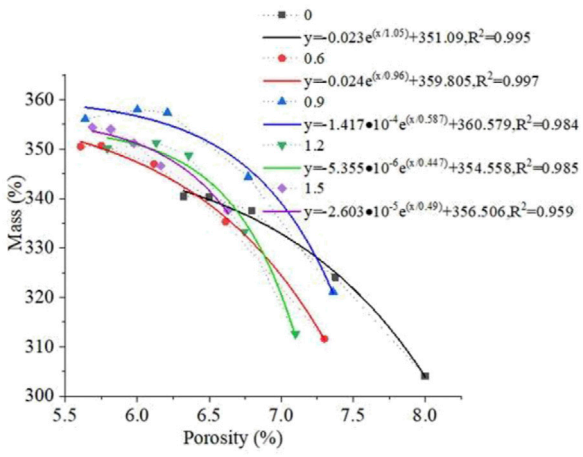

FIGURE 12
Curves fitting the relationship between porosity and change in mass.

The mass loss for each specimen gradually increased with unilateral salt freezing. Compared with the specimens prior to being subjected to freezing, after 40 FTCs, the maximum mass loss of 19.03% occurred in the specimen with no basalt fiber, and the minimum loss of mass of 6.56% occurred in the specimen with 1.5 kg/m^3 basalt fiber content. Compared with the specimens without basalt fiber, the mass loss was reduced by 20.23%, 50.74%, 20.06%, and 65.53% for the specimens with 0.6 kg/m^3, 0.9 kg/m^3, 1.2 kg/m^3, and 1.5 kg/m^3 basalt fiber content, respectively. As can be observed, the incorporation of basalt fiber can reduce the mass loss occurring in cement mortar under exposure to freeze–thaw action.

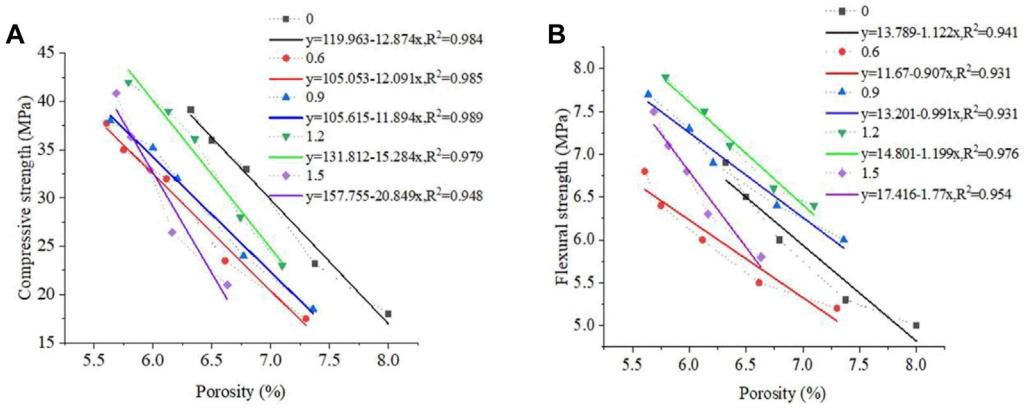

FIGURE 13
Curves fitting the relationship between porosity and **(A)** compressive strength; **(B)** flexural strength.

The equations fitting internal porosity variation to the mass loss of the specimens are shown in Figure 12. The pattern of variation of internal porosity with mass under unilateral salt freezing revealed a strong exponential change relationship for the specimens with 0 kg/m^3, 0.6 kg/m^3, 0.9 kg/m^3, 1.2 kg/m^3, and 1.5 kg/m^3 basalt fiber content, and the goodness of fit, R^2, was above 0.959 when the exponential equation was used. This result indicates that the action of unilateral salt freezing leads to the generation of internal damage inside the structure, which increases porosity more critically than erosion at the specimen surface and causes loss of mass.

3.6 Correlation between porosity and mechanics

The compressive and flexural strength values gradually reduced, and the internal porosity gradually increased when the specimens with basalt fiber content were subjected to unilateral salt freezing. Specimens with basalt fiber content of 1.2 kg/m^3, 1.5 kg/m^3, 0.9 kg/m^3, 0.6 kg/m^3, and 0 kg/m^3 correspond to the changes of the compressive and flexural strength values from large to small after 40 FTCs. Hence, comparing the change of mechanical properties and porosity suggests a correlation between the mechanical properties and microscopic pore structure characteristics.

The unit mass of the specimen without basalt fiber contained the highest degree of porosity, and its mechanical properties and durability were relatively bad under unilateral salt freezing. The porosity increase in specimens with basalt fiber was relatively slow, and the mechanical properties were enhanced after unilateral freezing. The increment was the smallest for the second and third peaks of the T2 spectrum of the specimens with basalt fiber content of 1.2 kg/m^3 and 1.5 kg/m^3, and the compressive and flexural strengths of those specimens were better. As a result, it is apparent that there is a certain correlation between the change of the internal pores and the change in the mechanical properties of the material under freeze–thaw action. Therefore, the variation of the internal porosity with the compressive and flexural strength can be fitted using a mathematical equation. The fitting results of the basalt-fiber-reinforced cement mortar specimens under unilateral salt freezing are shown in Figure 13.

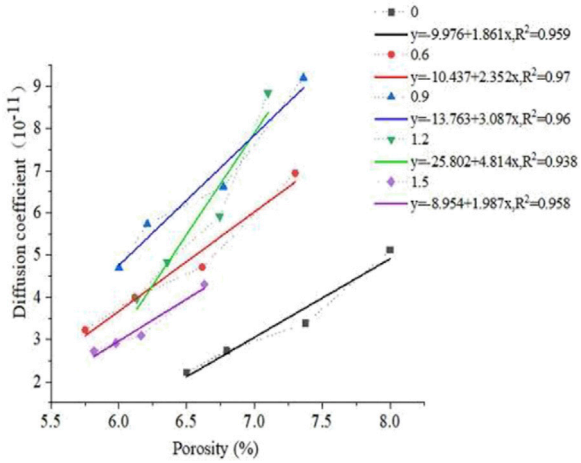

FIGURE 14
Fitting curve of chloride ion diffusion coefficient changes with porosity.

The growth of the porosity inside the mortar yielded a good negative linear correlation with the change of the compressive and flexural strength of the mortar for the specimens with a basalt fiber content of 0 kg/m^3–1.5 kg/m^3 under unilateral salt freezing. Thus, it can be concluded that the porosity inside the mortar will increase under the action of hydrostatic pressure, expansion pressure, and salt crystallization pressure caused by unilateral salt freezing, resulting in internal damage to the microstructure of the concrete. This internal structural damage is directly related to the compressive and flexural strength of the mortar and indicates that the increase in the porosity will directly and negatively affect the macroscopic mechanical properties of the mortar.

3.7 Correlation between porosity and chloride ion diffusion

Internal porosity and chloride ion diffusion coefficient both increased with an increase in the number of FTCs, as can be

ascertained from the previous analysis. Curves fitting the relationship between internal porosity and chloride ion diffusion coefficient for basalt-reinforced mortar under exposure to unilateral salt freezing are illustrated in Figure 14.

The growth of porosity within the specimens exhibited a strong positive linear correlation with the change in the chloride ion diffusion coefficient for cement mortar with 0–1.5 kg/m^3 basalt fiber content under exposure to unilateral salt freezing. This outcome demonstrates that internal porosity increases under exposure to continual unilateral salt freezing cycles, and internal microstructure damage resulted in an increase in chloride ion diffusion coefficients for the specimens under these conditions. As a result, the ability of the mortar to resist chloride ion erosion under freeze–thaw conditions will be gradually reduced and this will have a serious impact on the durability and safety of concrete structures.

Based on a comparison of the variation in chloride ion concentration and porosity characteristics, it can be argued that there are two main factors influencing the speed of chloride ion diffusion in cement: the porosity of the structure and the interface transition zone (ITZ) in the structure (Xu, 2018). Interestingly, the incorporation of fibers may increase the ITZ in the mortar, and exposure to unilateral freezing action could increase the internal porosity of the mortar. Therefore, considering the impact of these two aspects, we can explain the fact that, although porosity was higher in the mortar without basalt fibers than in the specimens with basalt fiber, the internal chloride ion concentration and diffusion coefficients were lower. A comparison of the changes in the porosity in the mortar with no basalt fibers and the mortar with 1.5 kg/m^3 basalt fiber content shows that although porosity per unit mass and the three peaks of the T2 spectrum were both higher for the specimen without basalt fiber than for those with 1.5 kg/m^3 basalt fiber content, the chloride ion diffusion coefficient was similar for each of these specimens. This result demonstrates that the influence of internal porosity and fiber content should be comprehensively considered in studying the diffusion coefficients of chloride ions for mortar with incorporated fiber.

4 Conclusion

Incorporation of basalt fiber at a content ratio ranging from 0 kg/m^3–1.5 kg/m^3 into normal Portland cement mortar can improve the compressive and flexural strength of cement mortar after a standard curing period of 7 d–28 d and under exposure to unilateral salt freezing. The optimum basalt fiber content was determined to be 1.2 kg/m^3. Changes in the compressive and flexural strength of basalt-reinforced cement mortar showed a linear relationship with the number of FTCs, and that showed cubic parabolic relationship with basalt fiber content.

The resistance of the properties of basalt-fiber-reinforced cement mortar to chloride ion diffusion may be affected both by its internal porosity characteristics and also by the interface transition zone within the structure. The variation in the chloride ion diffusion in cement mortar conforms to Fick's second law under exposure to unilateral salt freezing, and the diffusion coefficients show exponential growth with the number of FTCs.

Use of an appropriate level of basalt fiber content in cement mortar can reduce the internal damage caused by unilateral salt freezing. The porosity of the internal structure increases under continual exposure to unilateral salt freezing. The increase in micro- and transition pores within the structure was not found to be significant, but the increase in medium pores, macropores, and cracks was notable and had a major impact on the mechanical properties of the material.

Exposure to the continual action of FTCs will lead to the detachment of the basalt fiber and cement-based interface. This effect will result in a decline in compressive and flexural strength and in an increase in the chloride ion diffusion coefficient. As a result, the mechanical properties will deteriorate, and the related physical properties of cement mortar under will be negatively affected under exposure to FTCs.

In this study, the change in porosity within the structure exhibited an exponential relationship with the change in mass. Additionally, linear change was observed for the changes in the compressive strength, flexural strength, and chloride ion diffusion coefficient for basalt fiber-reinforced cement mortar under exposure to unilateral salt freezing.

The effects of basalt fiber length, size of cement mortar specimens, cement ratio, and aggregation ratio were not examined in this study, and the mechanisms underlying damage to basalt-fiber-reinforced cement material need to be further studied.

Data availability statement

The original contributions presented in the study are included in the article/supplementary material; further inquiries can be directed to the corresponding author.

Author contributions

JZ: investigation; writing—original draft; writing—review and editing. GW: conceptualization and methodology. GZ: conceptualization and methodology. All authors contributed to the article and approved the submitted version.

Funding

This research was funded by the Science and Technology Development Planning Project of Jilin Province of China, grant number 20230203039SF.

Conflict of interest

The authors declare that the research was conducted in the absence of any commercial or financial relationships that could be construed as a potential conflict of interest.

Publisher's note

References

Ahmed, W., and Lim, C. W. (2021). Production of sustainable and structural fiber reinforced recycled aggregate concrete with improved fracture properties: A review. *J. Clean. Prod.* 279, 123832. doi:10.1016/j.jclepro.2020.123832

Ahmad, M. R., and Chen, Bing (2018). Effect of silica fume and basalt fiber on the mechanical properties and microstructure of magnesium phosphate cement (MPC) mortar. *Constr. Build. Mater.* 190, 466–478. doi:10.1016/j.conbuildmat.2018.09.143

Cao, W. (2013). *Chloride transport and cover protection of concrete under drying-wetting cycles*. Xi'an: Xi'an University of Architecture & Technology.

Chen, F., Xu, B., Jiao, H., Chu, H., Wang, Y., and Liu, J. (2021). Fiber distribution and pore structure characterization of basalt fiber reinforced concrete[J]. *J. ChinaUniversity Min. Technol.* 50 (2), 273–280. doi:10.13247/j.cnki.jcumt.001260

Dhand, V., Mittal, G., Rhee, K. Y., Park, S. J., and Hui, D. (2015). A short review on basalt fiber reinforced polymer composites. *Compos. B* 73, 166–180. doi:10.1016/j.compositesb.2014.12.011

Dong, R., Shen, X., Xue, H., and Liu, Q. (2020). Sulfate resistance mechanism of aeolian sand concrete under dry-wet cycles. *Mater. Rep.* 34, 24040–24044.

Fiore, V., Scalici, T., Bella, G. D., and Valenza, A. (2015). A review on basalt fibre and its composites. *Compos. B* 74, 74–94. doi:10.1016/j.compositesb.2014.12.034

GB/T 50082-2009 (2019). *Standard of test methods of long-term performance and durability of ordinary concrete*. Beijing, China: Architecture & Building Press.

GB/T50081-2019 (2019). *Standard for test methods of concrete physical and mechanical properties*. Beijing, China: China Architecture & Building Press.

Gencel, O., Nodehi, M., Yavuz Bayraktar, O., Kaplan, G., Benli, A., Gholampour, A., et al. (2022). Basalt fiber-reinforced foam concrete containing silica fume: An experimental study. *Constr. Build. Mater.* 326, 126861. doi:10.1016/j.conbuildmat.2022.126861

Hong, L., Lin, J., Lei, X., and Wei, T. (2022). Compressive strength prediction of basalt fiber reinforced concrete via random forest algorithm. *Mater. Today Commun.* 30, 103117. doi:10.1016/j.mtcomm.2021.103117

Hu, X., Peng, G., and Niu, D. T. Y, C. (2020). Study of the stress-strain response of concrete during construction under repeated compressive loading. *J. Build. Mater.* 23, 1061–1070.

JamesHaido a, H., Tayeh, B. A., Majeed, S. S., and Karpuzcu, Mehmet (2021). Effect of high temperature on the mechanical properties of basalt fibre self-compacting concrete as an overlay material. *Constr. Build. Mater.* 268, 121725. doi:10.1016/j.conbuildmat.2020.121725

Jiao, H., Han, Z., Chen, X., Yang, Y., and Wang, Y. (2019). Flexural toughness evolution of basalt fiber reinforced shotcrete based on NMR technology[J]. *J. China Coal Soc.* 44 (10), 2990–2998.

Katkhuda, H., and Shatarat, N. (2017). Improving the mechanical properties of recycled concrete aggregate using chopped basalt fibers and acid treatment. *Constr. Build. Mater.* 140, 328–335. doi:10.1016/j.conbuildmat.2017.02.128

Khan, M., and Cao, M. (2021). Effect of hybrid basalt fibre length and content on properties of cementitious composites. *Mag. Concr. Res.* 73 (10), 487–498. doi:10.1680/jmacr.19.00226

Khan, M., Cao, M., Xie, C., and Ali, M. (2021). Efficiency of basalt fiber length and content on mechanical and microstructural properties of hybrid fiber concrete. *Fatig & Fract. Eng. Mater. Struct.* 44 (8), 2135–2152. doi:10.1111/ffe.13483

Kizilkanat, A. B., Kabay, N., Akyüncü, V., Chowdhury, S., and AbdullahAkça, H. (2015). Mechanical properties and fracture behavior of basalt and glass fiber reinforced concrete: An experimental study. *Constr. Build. Mater.* 100, 218–224. doi:10.1016/j.conbuildmat.2015.10.006

Lu, Y., Wang, L., Ge, Z., Zhou, Z., Deng, K., and Zuo, S. (2019). Fracture and pore structure dynamic evolution of coals during hydraulic fracturing. *Fuel* 10, 116272. doi:10.1016/j.fuel.2019.116272

Pehlivanlı, Z. O., Uzun, I., and Demir, I. (2015). Mechanical and microstructural features of autoclaved aerated concrete reinforced with autoclaved polypropylene, carbon, basalt and glass fiber. *Constr. Build. Mater.* 96, 428–433. doi:10.1016/j.conbuildmat.2015.08.104

Qiu, J. S., Song, H. T., Guan, X., Zhou, Y. X., and Fu, B. W. (2020). Damage evolution law of coal gangue concrete under the action of salt-freezing cycle. *Non-Met. Mines* 43, 28–32. doi:10.3969/j.issn.1000-8098.2020.01.008

Rambo, D. A. S., Silva, F. D. A., Filho, R. D. T., and da Fonseca Martins Gomes, O. (2015). Effect of elevated temperatures on the mechanical behavior of basalt textile reinforced refractory concrete. *Mater. Des.* 65, 24–33. doi:10.1016/j.matdes.2014.08.060

Su, L., Niu, D., Huang, D., and Fu, Q. (2022). Chloride diffusion performance of basalt/polypropylene fiber reinforced concrete in marine environment [J]. *J. Build. Mater.* 25 (1), 44–53. doi:10.3969/j.issn.1007-9629.2022.01.007

Sun, X., Gao, Z., Cao, P., and Zhou, C. (2019). Mechanical properties tests and multiscale numerical simulations for basalt fiber reinforced concrete. *Constr. Build. Mater.* 202, 58–72. doi:10.1016/j.conbuildmat.2019.01.018

Wu, Q., Ma, Q., and Wang, Y. (2021). Compression-tensile tests and meso-structure of basalt fiber-slag powder-fly ash concrete under freeze-thaw cycles [J]. *Acta Mater. Compos. Sin.* 38 (3), 953–965. doi:10.13801/j.cnki.fhclxb.20200722.002

Xiaoping, S. U. (2013). "Research on the concrete durability due to salinized soil in the Western region of Jilin province," in *Jilin uni-versity-China* (China: Changchun).

Xing, B. Y., Cheng, P. Y., Tang, J. P., Xie, E. H., Zeng, Q., and Zhou, C. S. (2021). Pore structure evolution of water-saturated mortar under freeze-thaw cycles. *J. Chin. Ceram. Soc.* 49, 331–339. doi:10.14062/j.issn.0454-5648.20200398

Xiong, Z., Mai, G., Qiao, S., He, S., Zhang, B., Wang, H., et al. (2022). Fatigue bond behaviour between basalt fibre-reinforced polymer bars and seawater sea-sand concrete. *Ocean Coast. Manag.* 218, 106038. doi:10.1016/j.ocecoaman.2022.106038

Xu, J. (2018). *Multi-scale study on chloride penetration in concrete under sustained axial pressure and marine environment[D]*. Xuzhou: China university of mining & technology.

Xue, W., Liu, X., Yao, Z., Hua, C., and Li, H. (2020). Effects of different damage sources on pore structure change characteristics of basalt fiber reinforced concrete. *Acta Mater. compos. Sin.* 37, 2285–2293. doi:10.13801/j.cnki.fhclxb.20200219.001

Yan, J., Zheng, J., and Li, N. (2019). Anti-cracking performance of asphalt mortar reinforced by basalt fiber[J]. *J. Build. Mater.* 22 (5), 800–804.

Yan, L. I. (2015). *Study on the physical and mechanical propertiesand damage mechanism of concrete mixed with mineral admixture in marine corrosion and freezing-thawing environment*. Xuzhou: China university of mining & technology.

Yang, L., Xie, H., Fang, S., Huang, C., Yang, A., and Yuh, J. (2021). Experimental study on mechanical properties and damage mechanism of basalt fiber reinforced concrete under uniaxial compression. *Structures* 31, 330–340. doi:10.1016/j.istruc.2021.01.071

Yavuz Bayraktar, O., Kaplan, G., Gencel, O., Benli, A., and Sutcu, M. (2021). Physico-mechanical, durability and thermal properties of basalt fiber reinforced foamed concrete containing waste marble powder and slag. *Constr. Build. Materials[J]* 288, 123128. doi:10.1016/j.conbuildmat.2021.123128

Ye, B., Jiang, J., Sun, W., and Wang, C. (2010). Innuence of basalt fiber on performances of mortar with mineral admixtures[J]. *J. Southeast Univ. Nat. Sci. Ed.* 40 (2), 34–39.

Zhang, C. S., Wang, Y. Z., Zhang, X. G., Ding, Y. H., and Xu, P. (2021). Mechanical properties and microstructure of basalt fiber-reinforced recycled concrete[J]. *J. Clean. Prod.* 278, 1–12. doi:10.1016/j.jclepro.2020.123252

Zhang, J., Wang, J., and Kong, D. (2010). Chloride diffusivity analysis of existing concrete based on Fick's second law. *J. Wuhan. Univ. Technol.-Mat. Sci. Ed.* 25, 142–146. doi:10.1007/s11595-010-1142-4

Zhao, Q., Dong, J., Pan, H., and Hao, S. (2010). Impact behavior of basalt fiber reinforced concrete[J]. *Acta Mater. Compos. Sin.* 27 (6), 120–125.

Zhou, H., Jia, B., Huang, H., and Mou, Y. (2020). Experimental study on basic mechanical properties of basalt fiber reinforced concrete. *Materials* 13 (6), 1362. doi:10.3390/ma13061362

Zhou, Y. X., Shen, X. D., and Li, G. F. (2018). Micropore of aeolian sand concrete under MgSO4-freeze-thaw cycles. *J. Build. Mater.* 21, 817–824.